Design-Ready Microwave Modeling by Spatial and Dimensional Domain Restriction

Slawomir Koziel[1,2][0000-0002-9063-2647], Anna Pietrenko-Dabrowska[2][0000-0003-2319-6782], and Leifur Leifsson[3][0000-0001-5134-870X]

[1] Engineering Optimization & Modeling Center, Department of Engineering, Reykjavík University, Menntavegur 1, 102 Reykjavík, Iceland
koziel@ru.is

[2] Faculty of Electronics Telecommunications and Informatics, Gdansk University of Technology, Narutowicza 11/12, 80-233 Gdansk, Poland
anna.dabrowska@pg.edu.pl

[3] School of Aeronautics and Astronautics, Purdue University, West Lafayette, IN 47907, USA
leifur@purdue.edu

Abstract. Surrogate modelling has become increasingly important in microwave engineering. Fast metamodels—particularly behavioral ones—are widely employed to accelerate design tasks such as parametric optimization by replacing costly full-wave electromagnetic (EM) simulations. However, constructing reliable surrogates remains challenging due to the strong nonlinearity of circuit responses and the curse of dimensionality. The difficulty is especially pronounced in design-oriented modeling, where validity must be ensured across wide ranges of parameters. This research introduces an innovative modeling procedure that combines dimensionality reduction with spatial domain restriction to reduce the training data acquisition cost while enhancing predictive accuracy. Dimensionality reduction is achieved using fast global sensitivity analysis, which determines the parameter-space directions with the strongest impact on the system's frequency characteristics. These vectors define the reduced domain, which is additionally confined by means of principal component analysis (PCA) of prescreened high-quality designs. As a result, the surrogate is concentrated on the relevant design space subsets, ensuring suitability for practical design tasks while maintaining high accuracy. The proposed methodology has been extensively validated against state-of-the-art benchmarks, demonstrating both competitive precision and significant efficacy gains. Its design readiness has been shown through practical applications, specifically, in EM-driven circuit optimization under varying specification scenarios.

Keywords: Microwave circuits, behavioral modeling, domain confinement, dimensionality reduction, sensitivity analysis.

1 Introduction

The design of high-frequency systems relies heavily on advanced simulation tools, such as circuit-level [1] and electromagnetic (EM) solvers [2]. EM analysis is indispensable for accurately capturing critical effects such as mutual coupling, substrate

ICCS Camera Ready Version 2026
To cite this paper please use the final published version:
DOI: 10.1007/978-3-032-29909-3_11

and radiation losses, and the influence of connectors. These phenomena play a key role in the performance of modern microwave circuits, from compact components [3] to structures incorporating metamaterials [4]. However, EM simulations are computationally intensive, which poses a major challenge in scenarios requiring repeated evaluations, such as parameter tuning [5], uncertainty quantification [6], and multi-objective optimization [7]. Among these, global search procedures are particularly costly, especially when employing bio-inspired algorithms [8]. To mitigate this, considerable research was directed towards accelerating EM-driven procedures. Established methods include adjoint sensitivity analysis [9], sparse Jacobian updating [10], mesh deformation [11], response feature technology [12], and model order reduction [13]. More recently, surrogate-assisted design has gained significant traction [14], [15], frequently implemented within machine learning (ML) frameworks [16]. Common surrogate modeling strategies encompass kriging [17], support vector regression [18], Gaussian process regression [19], and various neural network architectures [20]-[22].

Fast surrogate models can substantially reduce the cost of EM-driven design workflows, particularly in optimization tasks. However, constructing reliable metamodels remains challenging and often expensive. Key difficulties arise from the strong nonlinearity of circuit frequency responses, the need to cover broad ranges of design variables (to ensure practical applicability), and the curse of dimensionality [23]. Several strategies have been proposed to alleviate these issues. Some focus on improving the utilization of available data, such as ensemble learning [24]; others address efficient handling of large training sets through deep learning [25]. Still others exploit structural properties of system outputs, as in high-dimensional model representation (HDMR) [26]. Cost efficiency can also be improved by employing variable-resolution techniques, e.g., co-kriging [27]. An alternative is performance-driven modeling [28], in which the metamodel is built within a carefully defined subset containing high-quality designs. This approach can significantly improve predictive accuracy while preserving design relevance. Recently, domain confinement concepts have been extended to deep learning frameworks [29]. A limitation of such methods, however, is their restricted generality, since the reduced domain is typically defined with respect to specific performance requirements [28].

This paper introduces a new technique for high-efficacy and dependable behavioral modeling of microwave circuits. Our framework combines reducing the problem dimensionality, conducted by fast global sensitivity analysis (FGSA), with spatial domain restriction achieved via randomized parameter screening. FGSA identifies a low-dimensional subspace that captures the dominant variability in circuit responses, while pre-screening isolates the regions most relevant to high-quality designs. Together, these mechanisms enable the construction of accurate data-driven surrogates from relatively small training datasets. Comprehensive verification studies and benchmarking against a range of state-of-the-art techniques assert the competitive operation of the suggested methodology regarding predictive accuracy, computational efficiency, and scalability. Furthermore, its practical usefulness is demonstrated by practical engineering applications, focusing on circuit optimization under diverse setups, and supported by experimental validation of selected designs.

ICCS Camera Ready Version 2026
To cite this paper please use the final published version:
DOI: 10.1007/978-3-032-29909-3_11

2 Modeling Methodology

This section encapsulates an in-depth explanation of the proposed modeling approach. We formulate the modeling task in Section 2.1. Domain confinement using global sensitivity analysis and spatial reduction is covered in Section 2.2, whereas Section 2.3 summarizes the entire methodology.

2.1 Problem Formulation

The notation used throughout is explained in Fig. 1. We aim to construct a surrogate $\boldsymbol{R}_s(\boldsymbol{x})$ representing the high-resolution EM model $\boldsymbol{R}_f(\boldsymbol{x})$ within the subsets of interest and a chosen range of operating frequencies. $\boldsymbol{R}_f$ denotes a generic circuit response. In practice, we handle S-parameters, such as S_{11} through S_{41} in the case of coupling structures. The modeling reliability is quantified by a relative root-mean squared error (RRMSE), which is well-aligned with visual assessment of the model's prediction reliability. Models that exhibit RRMSE at the level of a few percent are generally suitable for design purposes.

2.2 Domain Confinement Using Global Sensitivity and Spectral Analysis

The main challenges in data-driven modeling of microwave components stem from response nonlinearity, the size of the parameter space, and high dimensionality (number of decision variables). All else being equal, the predictive accuracy of a model depends on the average distance between training samples, which increases unfavorably as dimensionality grows (typically beyond three or four variables). Therefore, reducing both dimensionality and parameter space volume is essential to improve surrogate accuracy and enhance the cost efficiency of the modeling process.

Dimensionality reduction can be approached through various techniques, including variable screening (e.g., [30]-[32]) and global sensitivity analysis (GSA), such as Sobol indices or regression-driven approaches [33]-[35]. However, these methods are computationally demanding, as they typically require generating large sets of random samples along with perturbation points.

Symbol	Description	Comments
$\boldsymbol{x} = [x_1 \ldots x_n]^T$	Vector of circuit parameters	Independent circuit dimensions to be tuned in the design process
$X = [\boldsymbol{l}\ \boldsymbol{u}]$	Conventional parameter space	$\boldsymbol{l} = [l_1 \ldots, l_n]^T$ and $\boldsymbol{u} = [u_1 \ldots, u_n]^T$ are lower and upper bounds on parameters, i.e., we have $l_k \le x_k \le u_k$ for $k = 1, \ldots, n$
$\boldsymbol{R}_f(\boldsymbol{x})$	High-fidelity model (generic response)	Responses of the high-fidelity EM simulation model of the circuit at hand. The symbol $\boldsymbol{R}_f(\boldsymbol{x})$ stands for aggregated circuit characteristics evaluated over the frequency range of interest, F
$S_{kj}(\boldsymbol{x},f)$	High-fidelity model (scattering parameters)	Scattering parameters as functions of the parameter vector $\boldsymbol{x}$ and frequency f; k and j stand for the circuit ports
$\boldsymbol{R}_s(\boldsymbol{x})$	Surrogate model	Responses of the surrogate model of the circuit of interest

Fig. 1. Notation used by proposed surrogate modeling methodology.

ICCS Camera Ready Version 2026
To cite this paper please use the final published version:
DOI: 10.1007/978-3-032-29909-3_11

Moreover, their application often results in discarding the least influential variables, which is not always desirable for high-frequency components, where circuit responses—particularly in compact devices—are strongly governed by the combined impact of multiple variables.

We employ the fast global sensitivity analysis (FGSA) technique originally introduced in [36]. FGSA identifies the influential parameter space directions concerning system response variations. These vectors define the domain of the metamodel. Importantly, the identified directions are generally misaligned with the coordinate axes, thereby enhancing the surrogate representation flexibility. To extract these directions, circuit response variations are evaluated for pairs of randomly generated designs uniformly distributed across the parameter space. From these variations, a relocation matrix $\boldsymbol{S}$ is constructed and subjected to spectral decomposition using prinicipal component analysis (PCA). The resulting eigenvectors $\boldsymbol{e}_j$ correspond to the main directions of response variability, with their importance evaluated by the associated eigenvalues λ_j, $j = 1, \ldots, n$. The reduced region X_d is formed by the N_d most significant eigenvectors, selected according to the condition $\| [\lambda_1 \ldots \lambda_{Nd}]^T \| / \| [\lambda_1 \ldots \lambda_n]^T \| \geq C_{\min}$ where $C_{\min} = 0.9$ (as recommended in [36]). Although the dimensionality of X_d is lower than the original n, it retains the dominant sources of response variability, ensuring that neglecting the remaining $n - N_d$ directions does not jeopardize the design relevance of the model.

The domain is determined in two steps. We begin by FGSA-based dimensionality reduction. More specifically, we use N_d eigenvectors $\boldsymbol{e}_j$, $j = 1, \ldots, N_d$, to define

$$X_d = \left\{ \boldsymbol{x} \in X : \boldsymbol{x} = \boldsymbol{x}_c + \sum_{j=1}^{N_d} a_j \boldsymbol{e}_j \right\}, \quad \boldsymbol{x}_c = [\boldsymbol{l} + \boldsymbol{u}]/2 \tag{1}$$

where the spanning factors are marked as a_j, $j = 1, \ldots, N_d$. Figures 2(a) and 2(b) provide a graphical illustration of X_d. It should be reiterated that while $N_d < n$, the set X_d captures the directions responsible for the most influential share of response variations. Consequently, excluding other directions does not diminish the design usefulness of the metamodel built within this reduced space.

The second step in defining the domain involves volume reduction, achieved through quality-driven pre-screening. In this stage, regions of X_d containing high-quality designs are identified. For instance, in coupling or power-dividing circuits, desirable performance corresponds to a good reflection coefficient level and port isolation, and appropriate power division ratios.

Let $Q(\boldsymbol{x})$ be a design merit assessment function, with $Q(\boldsymbol{x}) = 1$ for acceptable parameter vectors (e.g., for which $|S_{11}|, |S_{41}| \leq -20$ dB at the center frequency), and $Q(\boldsymbol{x}) = 0$ for poor-quality vectors. Let $\boldsymbol{x}_q^{(j)} \in X_d$, $j = 1, \ldots, N_q$, be a set of random samples (typically, $N_q = 50$), and $\boldsymbol{x}_r^{(j)}$, $j = 1, \ldots, N_r$, is a subset of $\{\boldsymbol{x}_q^{(j)}\}_{j=1,\ldots,Nq}$, so that $Q(\boldsymbol{x}_r^{(j)}) = 1$ for all $j \in \{1, \ldots, N_r\}$. The set $\{\boldsymbol{x}_r^{(j)}\}$ is employed to identify the volume-confined domain as follows. Given $\boldsymbol{x}_m = N_r^{-1} \sum_{j=1,\ldots,Nr} \boldsymbol{x}_r^{(j)}$ (the center of $\{\boldsymbol{x}_r^{(j)}\}$), a covariance matrix is assembled

$$\boldsymbol{S}_r = \frac{1}{N_r - 1} \sum_{j=1}^{N_r} (\boldsymbol{x}_r^{(j)} - \boldsymbol{x}_m)(\boldsymbol{x}_r^{(j)} - \boldsymbol{x}_m)^T \tag{2}$$

Spectral analysis of $\boldsymbol{S}_r$ yields the eigenvectors $\boldsymbol{a}_k$, $k = 1, \ldots, N_d$. Note that the vectors $\{\boldsymbol{a}_k\}_{k = 1, \ldots, Nd}$, form an orthogonal basis in X_d. Consequently, each $\boldsymbol{x}_r^{(j)}$ has a unique expansion

ICCS Camera Ready Version 2026
To cite this paper please use the final published version:
DOI: 10.1007/978-3-032-29909-3_11

$$\boldsymbol{x}_r^{(j)} = \sum_{k=1}^{N_d} b_{jk}\boldsymbol{a}_k \tag{3}$$

Based on b_{jk}, we additionally define $b_{j.\max} = \max\{k : b_{kj}\}$, $b_{j.\min} = \min\{k : b_{kj}\}$ $b_{j.0} = (b_{j.\min} + b_{j.\max})/2$, for $j = 1, \ldots, N_s$, $\boldsymbol{b}_0 = [b_{1.0} \ldots b_{Nd.0}]^T$, and $\boldsymbol{l}_b = [l_{b1} \ldots l_{bNb}]^T$, where $l_{bj} = (b_{j.\max} - b_{j.\min})/2$. Further, we set $\boldsymbol{x}_b = \boldsymbol{x}_m + \boldsymbol{A}\boldsymbol{b}_0$, where $\boldsymbol{A} = [\boldsymbol{a}_1 \ldots \boldsymbol{a}_{Nd}]^T$ is an $n \times N_d$ matrix. The minimum N_d-dimensional interval encapsulating vectors $\boldsymbol{x}_r^{(j)}$, $j = 1, \ldots, N_r$ is

$$X_b = \left\{ \begin{array}{c} \boldsymbol{x} = \boldsymbol{x}_b + \sum_{k=1}^{N_d} (2c_k - 1) l_{b_k} \boldsymbol{a}_k \\ 0 \le c_k \le 1, \;\; k = 1, \ldots, N_d \end{array} \right\} \tag{4}$$

X_b is the subset of the subspace $\boldsymbol{x}_c + \Sigma_{j=1,\ldots,Nd} a_j \boldsymbol{e}_j$ encapsulating better-quality parameter vectors as assessed by $Q(\boldsymbol{x})$.

Now, the ultimate surrogate model domain is $X_S = X_d \cap X_b$ (see Fig. 2(c) for a visual illustration). The metamodel is rendered X_S using kriging [37]. In this study, the particular modelling method is of secondary concern because we primarily aim at investigating the advantages of restricting both dimensionality and volume.

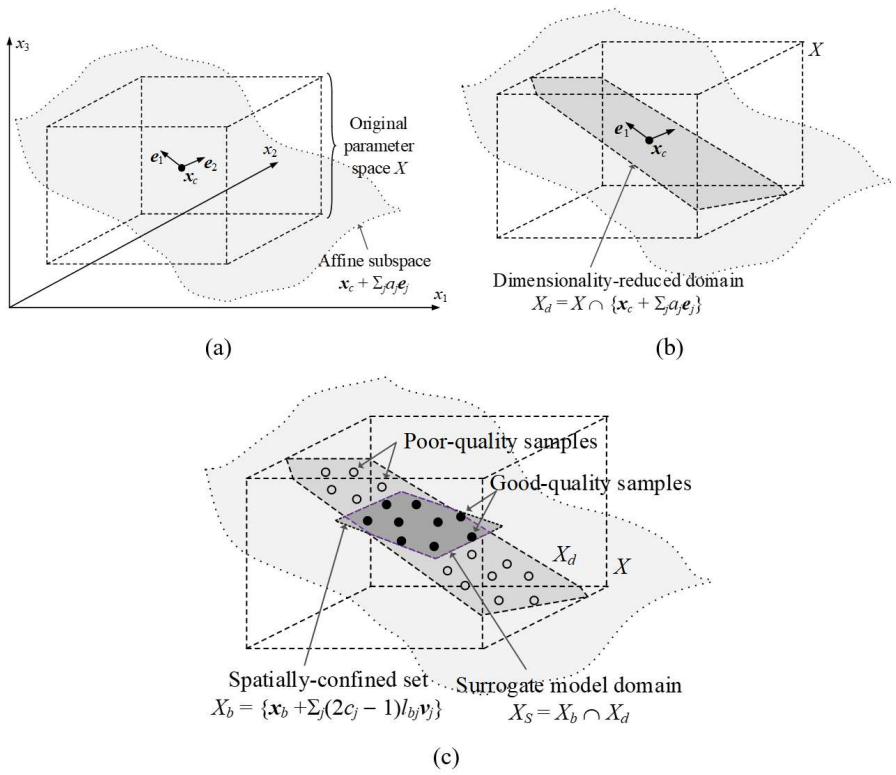

Fig. 2. Dimensionally- and spatially-restricted model domain X_S: (a) conventional design variable space X (illustrated for a three-dimensional case), and the subspace $\boldsymbol{x}_c + \Sigma_{j=1,2}\, a_j \boldsymbol{e}_j$ spanned by $N_d = 2$ eigenvectors $\boldsymbol{e}_1$ and $\boldsymbol{e}_2$; (b) restricted domain X_d, defined as an intersection of X and the affine space of Fig. 2(a); (c) volume-wise restricted subset X_b, and the ultimate region of interest $X_S = X_d \cap X_b$.

ICCS Camera Ready Version 2026
To cite this paper please use the final published version:
DOI: 10.1007/978-3-032-29909-3_11

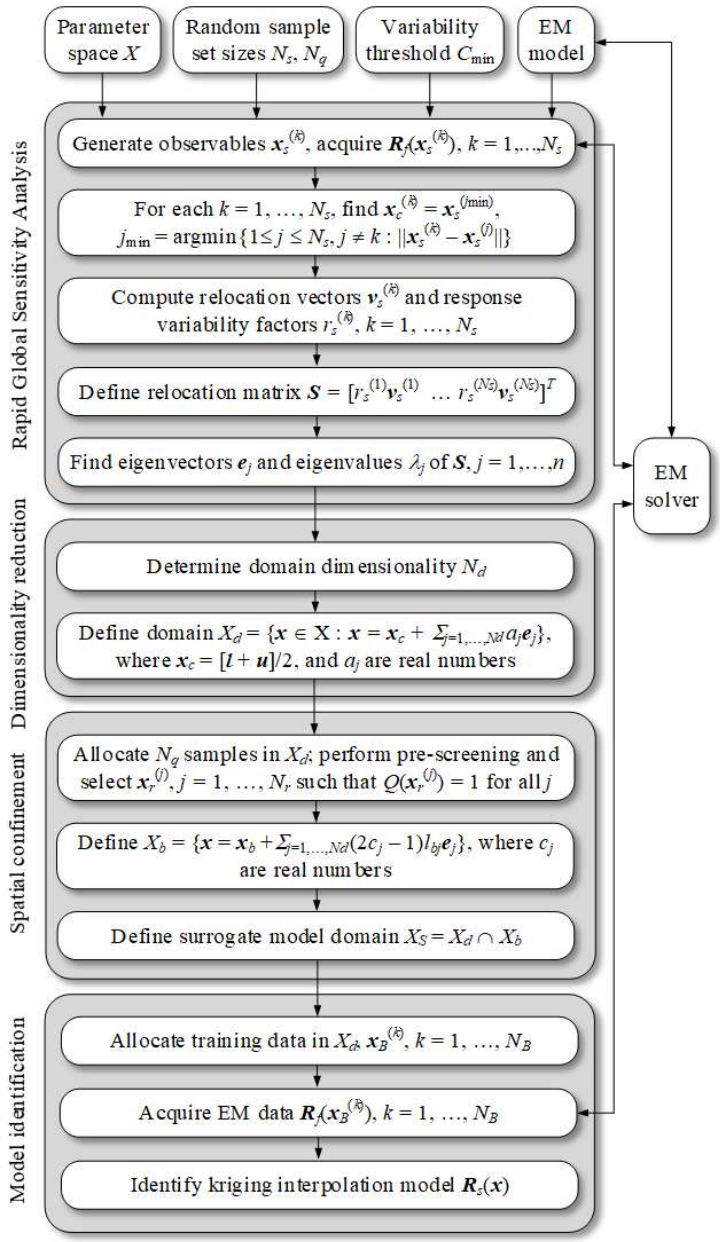

Fig. 3. Proposed modeling methodology: the block diagram.

ICCS Camera Ready Version 2026
To cite this paper please use the final published version:
DOI: 10.1007/978-3-032-29909-3_11

2.3 Modeling Procedure

The complete modelling framework incorporates the steps elucidated in Section 2.2. The first stage is global sensitivity analysis, followed by dimensionality restriction and spatial confinement. The restricted region is populated using training samples, and the EM data is collected. The last stage is model identification, where we use kriging interpolation. The block diagram of the procedure is included in Fig. 3. One of the benefits of our technique is a limited number of control parameters, including the threshold $C_{\min}$ (default value of 0.9) and the amount of random points N_s used by FGSA, as well as the number of N_q of pre-screening vectors employed by the spatial confinement (both numbers are set to $N_s = N_q = 50$).

3 Results

This section presents numerical and experimental validation of the suggested modeling procedure based on two planar circuits and several state-of-the-art benchmark techniques.

3.1 Verification Circuits. Algorithm Setup and Benchmark Methods

Figure 4 shows the microwave structures used for verification and their essential characteristics. The EM representations are evaluated in CST Microwave Studio. Our surrogate was rendered in the restricted domain established using FGSA with $N_s = 50$ random samples. The domain dimensionality N_d was established using the variability threshold $C_{\min} = 0.9$ (cf. Section 2). For Circuit I, we have $N_d = 3$, whereas for Circuit II, $N_d = 4$. The surrogate models are built using training ensembles of diverse sizes between 50 and 800 samples (also, 1,600 samples for Circuit II). The data-driven modelling approach is kriging interpolation with Gaussian correlation functions. Our approach is juxtaposed against state-of-the-art benchmark methods outlined in Table 1.

3.2 Results and Discussion

The outcomes are summarized in Tables 2 and 3. The surrogate-predicted versus EM-evaluated frequency characteristics at representative test points are illustrated in Figs. 5 and 6. As indicated in the tables, combining dimensionality reduction with spatial domain confinement substantially improves both the predictive accuracy and computational efficiency of the surrogate models. The key findings can be outlined as follows:

- Surrogates in the baseline space X exhibit high error levels, confirming the difficulty of the test problems considered. In the case of Circuit I, almost all methods reduce RRMSE below 10% with datasets sets of 400–800 samples. However, for Circuit II, typical errors remain at 20% or higher, even with 1,600 samples, rendering such models impractical.
- The proposed modeling framework delivers substantial accuracy gains. For Circuit I, errors fall below 5% with as few as 50 training samples. For Circuit II, an error of ~8% is achieved with 800 samples, further reduced to ~6% with 1,600

ICCS Camera Ready Version 2026
To cite this paper please use the final published version:
DOI: 10.1007/978-3-032-29909-3_11

samples. On average, for 800-sample sets, our approach yields surrogates that are 5.4 times more accurate (Circuit I) and 3.7 times more accurate (Circuit II) than benchmarks constructed in the full-dimensional space.

- Spatial reduction significantly enhances model accuracy. When compared with the best-performing benchmark method (kriging in the reduced parameter space X_d), the proposed approach achieves an average error reduction of about a multiplicative factor of 1.3 across all training set sizes and both circuits.

A key practical benefit of the suggested methodology is its capability to construct reliable models even from relatively small training sets. For Circuit I, this is possible with just 50 samples. For Circuit II—the most challenging case—a usable surrogate is obtained with 800 samples. By contrast, benchmark models perform substantially worse across all configurations.

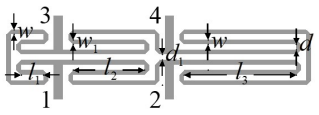

Parameter	Description
Substrate	RO4003 (ε_r = 3.38, h = 0.762 mm)
Design parameters	$\boldsymbol{x} = [l_1\ l_2\ l_3\ d\ w\ w_1]^T$
Conventional parameter space X	$\boldsymbol{l} = [2.0\ 7.0\ 12.5\ 0.2\ 0.7\ 0.2]^T$, $\boldsymbol{u} = [4.5\ 12.5\ 22.0\ 0.65\ 1.5\ 0.9]^T$
Modelled characteristics	S-parameters S_{11}, S_{21}, S_{31}, S_{41}
Frequency range	0.5 GHz to 2.5 GHz

(a)

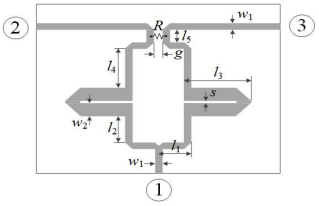

Parameter	Description
Substrate	AD250 (ε_r = 2.5, h = 0.81 mm)
Design parameters	$\boldsymbol{x} = [l_1\ l_2\ l_3\ l_4\ l_5\ s\ w_2]^T$
Conventional parameter space X	$\boldsymbol{l} = [14.5\ 1.1\ 13.0\ 0.5\ 1.6\ 0.19\ 3.9]^T$, $\boldsymbol{u} = [37.0\ 16.6\ 35.0\ 15.0\ 5.6\ 1.5\ 5.8]^T$
Modelled characteristics	S-parameters S_{11}, S_{21}, S_{31}, S_{22}, S_{33}, S_{32}
Frequency range	0.5 GHz to 7.0 GHz

(b)

Fig. 4. Test circuits: (a) miniaturized rat-race coupler [38], (b) dual-band power divider [39]. Circuit dimensions are in millimeters.

Table 1. Benchmark approaches

Modeling technique	Model setup
Kriging interpolation	• Gaussian correlation function • Second-order polynomial as a trend function
Radial basis functions	• Gaussian correlation functions • Scaling coefficient determined using cross-validation
Artificial neural network (ANN)	• Feedforward network with two hidden layers • Model training: backpropagation
Convolutional neural network (CNN)	• Uses four filters with filter sizes of [64 128 256 512] • Model training: ADAM algorithm
Ensemble learning	• Uses least-squares boosting with 250 learning cycles • Learning rate adjusted through Bayesian optimization
Kriging interpolation	• Domain established using FGSA with the same setup as for the proposed approach (N_s = 50, $C_{\min}$ = 0.9) • Gaussian correlation functions; second-order polynomial as a trend function

ICCS Camera Ready Version 2026
To cite this paper please use the final published version:
DOI: 10.1007/978-3-032-29909-3_11

Table 2. Results for Circuit I (error metric: RRMSE)

Modeling method	Number of training samples				
	50	100	200	400	800
Kriging	25.7 %	17.9 %	13.5 %	9.9 %	8.0 %
RBF	28.3 %	19.1 %	13.9 %	10.3 %	8.9 %
ANN	18.2 %	12.2 %	8.0 %	7.8 %	6.5 %
CNN	22.9 %	12.7 %	8.0 %	5.5 %	4.5 %
Ensemble learning	32.7 %	28.1 %	25.0 %	22.8 %	19.1 %
Kriging in dimensionality-reduced domain X_d	5.9 %	3.8 %	2.8 %	2.4 %	1.8 %
Kriging in dimensionality-reduced and spatially-confined domain X_S [this work]	4.1 %	3.2 %	2.4 %	2.1 %	1.5 %

Table 3. Results for Circuit II (error metric: RRMSE)

Modeling method	Number of training samples					
	50	100	200	400	800	1,600
Kriging	63.6 %	53.8 %	45.2 %	40.0 %	35.1 %	32.3 %
RBF	68.9 %	55.2 %	43.9 %	40.8 %	37.2 %	33.3 %
ANN	36.7 %	33.2 %	24.6 %	20.8 %	20.3 %	19.5 %
CNN	89.6 %	44.7 %	26.0 %	17.8 %	15.8 %	14.2 %
Ensemble learning	47.8 %	40.6 %	38.1 %	36.2 %	33.6 %	30.9 %
Kriging in dimensionality-reduced domain X_d	38.9 %	28.7 %	23.5 %	16.6 %	12.5 %	8.4 %
Kriging in dimensionality-reduced and spatially-confined domain X_S [this work]	32.8 %	24.2 %	15.2 %	12.1 %	8.5 %	6.0 %

3.1 Application Case Studies. Experimental Validation

As shown in Section 3.2, the proposed modeling framework achieves excellent performance by combining dimensionality reduction with performance-driven spatial confinement. To validate that these improvements do not compromise practical design utility, this section presents application case studies. Specifically, we optimize the test circuits under several design scenarios, outlined in Fig. 7. For each circuit, four sets of design specifications are considered. The key operating parameters are the center frequency f_0 and power division coefficient K_P for Circuit I, and the lower and upper operating frequencies (f_1, f_2) for Circuit II. The results are summarized in Tables 4 and 5, while Figs. 8 and 9 depict the frequency responses of the designs produced through the optimization of the proposed metamodel. In all cases, the agreement between metamodel-predicted EM-simulated characteristics is excellent, confirming the suitability of the presented modeling approach for real-world design tasks.

For additional validation, two representative designs (Case 2 for each circuit) were manufactured and experimentally tested. The measured outputs are compared with surrogate-based predictions and EM simulations in Fig. 10. The results demonstrate satisfactory agreement, with minor discrepancies attributable to fabrication tolerances, assembly imperfections, and connector effects.

ICCS Camera Ready Version 2026
To cite this paper please use the final published version:
DOI: 10.1007/978-3-032-29909-3_11

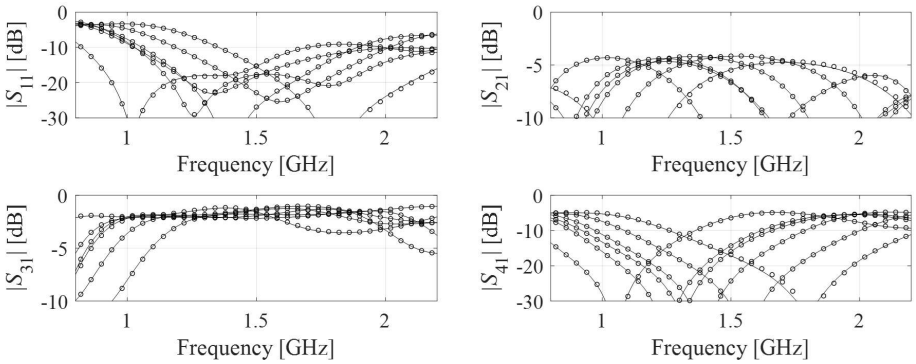

Fig. 5. Circuit I: *S*-parameters at the representative test points: EM analysis (—), and the presented surrogate rendered using 400 training samples (o).

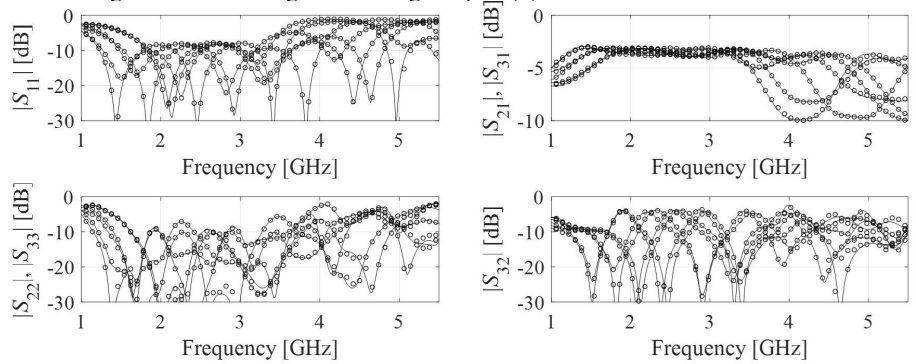

Fig. 6. Circuit II: *S*-parameters at the representative test points: EM analysis (—), and the presented surrogate rendered using 800 training samples (o).

Circuit	Design objectives
I	1. Minimize matching $\|S_{11}\|$ and isolation $\|S_{41}\|$ responses at the target operating frequency f_0; 2. Maintain target power split ratio $\|S_{31}\| - \|S_{21}\| = K_P$ at f_0.
II	1. Minimize input matching $\|S_{11}\|$ and output matching $\|S_{22}\| = \|S_{33}\|$ simultaneously at the target operating frequencies f_1 and f_2; 2. Minimize port isolation $\|S_{32}\|$ at both f_1 and f_2; 3. Maintain equal power division ratio, i.e., $\|S_{21}\| = \|S_{31}\|$ at f_1 and f_2.

§ Relative permittivity is one of the design variables of the modelling process.

Fig. 7. Design scenarios for the test circuits.

Table 4. Optimization outcomes for Circuit I

Case	Target operating conditions		Geometry parameter values [mm]					
	f_0 [GHz]	K_P [dB]	l_1	l_2	l_3	d	w	w_1
1	1.0	–3	3.62	9.7	21.4	0.32	1.48	0.48
2	1.5	0	2.95	10.7	14.2	0.63	0.86	0.76
3	2.0	–6	2.50	9.1	12.9	0.20	1.14	0.51
4	1.2	–3	3.42	9.3	18.7	0.35	1.16	0.44

ICCS Camera Ready Version 2026
To cite this paper please use the final published version:
DOI: 10.1007/978-3-032-29909-3_11

Table 5. Circuit II: Optimization outcomes for Circuit II

Case	Target operating conditions		Geometry parameter values [mm]						
	f_1 [GHz]	f_2 [GHz]	l_1	l_2	l_3	l_4	l_5	s	w_2
1	2.0	4.0	26.0	6.78	27.5	4.53	4.79	0.20	5.17
2	1.5	2.45	30.9	10.1	30.9	8.95	4.36	0.73	4.30
3	1.8	3.0	26.1	10.2	23.9	10.3	2.60	1.44	4.41
4	3.3	5.0	31.4	13.3	34.1	10.5	3.35	0.97	3.90

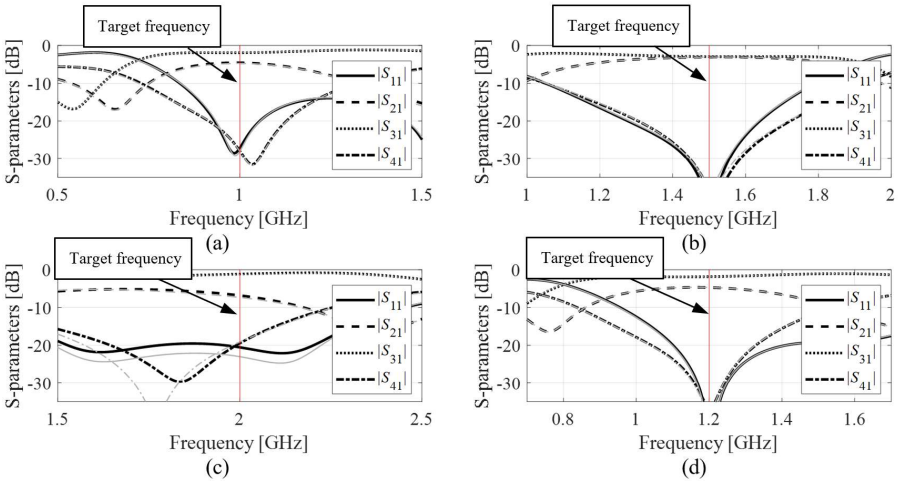

Fig. 8. Circuit I: model-predicted (gray) and EM-simulated responses (black) at the design generated through optimization of the proposed metamodel ($N_B = 400$): (a) Case 1, (b) Case 2, (c) Case 3, (d) Case 4.

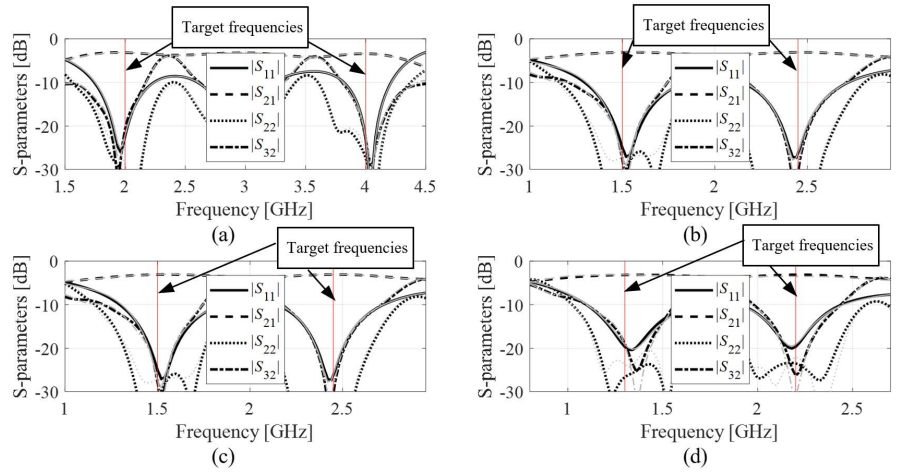

Fig. 9. Circuit II: model-predicted (gray lines) and EM-simulated responses (black lines) at the design generated by optimizing the proposed metamodel ($N_B = 800$): (a) Case 1, (b) Case 2, (c) Case 3, (d) Case 4.

ICCS Camera Ready Version 2026
To cite this paper please use the final published version:
DOI: 10.1007/978-3-032-29909-3_11

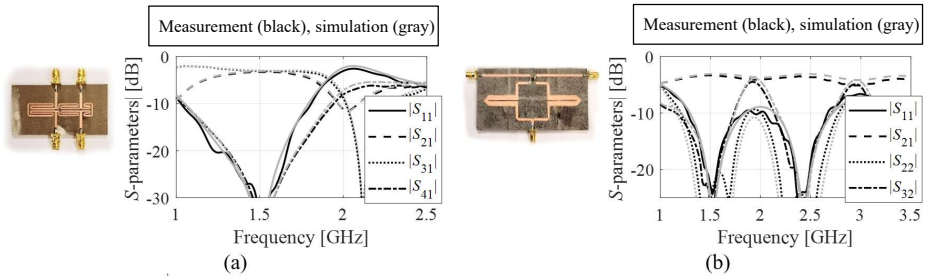

Fig. 10. Fabrication and measurements of selected designs optimized using the proposed metamodel: (a) Circuit I, (b) Circuit II.

4 Conclusion

This paper presented a high-precision methodology for behavioral modeling of passive microwave circuits. The technique integrates dimensionality restriction, achieved through fast global sensitivity analysis, with spatial reduction based on randomized prescreening. These mechanisms enable the development of highly accurate surrogate models from relatively small training datasets. The effectiveness of the suggested framework is showcased using two microstrip circuits. Extensive comparative studies highlight its superiority over multiple benchmark methods regarding predictive accuracy, computational efficiency, and scalability. In addition, application-oriented case studies confirm the practical design usefulness of the metamodels, which is further substantiated by experimental verification of representative optimized devices.

Acknowledgement

The authors would like to thank Dassault Systemes, France, for making CST Microwave Studio available. This work is partially supported by the Icelandic Research Fund Grant 239858 and by the National Science Centre of Poland Grant 2024/55/B/ST7/01413.

References

1. ADS (Advanced Design System), Keysight Technologies, Fountaingrove Parkway 1400, Santa Rosa, CA 95403-1799 (2024)
2. CST Microwave Studio, Dassault Systemes, Rue Marcel Dassault, 78140 Velizy-Villacoublay, France (2025)
3. Chen, J.-X., Xue, Y., Shi, X., Qin, W., Yang, Y.-J. Analysis and design of compact ridge waveguide bandpass filter and filtering balun with improved upper stopband performance. *IEEE Trans. Microwave Theory Techn.*, **73**, 3977–3986 (2025)
4. Arsanjani, A., Robins, L., Bartlett, C., Teschl, R., Höft, M., Bösch, W. The pixelated metasurface: a novel component design approach. *IEEE Trans. Microwave Theory Techn.*, **73**, 4021–4030 (2025)
5. Koziel, S., Pietrenko-Dabrowska, A., Reliability enhancement of EM-based tuning of microwave components using regularized operating band scanning. *Sc. Rep.*, **15**, paper no. 28000 (2025)

ICCS Camera Ready Version 2026
To cite this paper please use the final published version:
DOI: 10.1007/978-3-032-29909-3_11

6. Wang, Q., Li, P., Zhang, Y., Tan, G., Yang, Y., Rocca, P. Robust design and tolerance analysis of shaped reflector antennas based on interval analysis. *IEEE Ant. Wireless Propag. Lett. Letters*., **24**, 2392–2396 (2025)
7. Liu, S., Pei, C., Khan, L., Wang, H., Tao, S. Multiobjective optimization of coding metamaterial for low-profile and broadband microwave absorber. *IEEE Ant. Wireless Propag. Lett.*, **23**, 379–383 (2024)
8. Oyelade, O.N., Ezugwu, A.E.-S., Mohamed, T.I.A., Abualigah, L. Ebola optimization search algorithm: a new nature-inspired metaheuristic optimization algorithm. *IEEE Access*, **10**, 16150–16177 (2022)
9. Na, W., *et al.*, Advanced EM optimization using adjoint-sensitivity-based multifeature surrogate for microwave filter design. *IEEE Microwave Wireless Techn. Lett.*, **34**, 1–4 (2024)
10. Pietrenko-Dabrowska, A., Koziel, S., Computationally-efficient design optimization of antennas by accelerated gradient search with sensitivity and design change monitoring. *IET Microwaves Ant. Prop.*, **14**, 165–170 (2020)
11. Chen, S., Li, X., Zeng, Y., Tan, Y. A method for predicting radiation fields of deformed flexible antennas based on infinitesimal dipole model. *IEEE Trans. Ant. Propag.*, **73**, 6367–6380 (2025)
12. Pietrenko-Dabrowska, A., Koziel, S. Response feature technology for high-frequency electronics. Optimization, modeling, and design automation, Springer, New York (2023)
13. Zhang, J., Feng, F., Zhang, Q.-J. Rapid yield estimation of microwave passive components using model-order reduction based neuro-transfer function models. *IEEE Microwave Wireless Comp. Lett.*, **31**, 333–336 (2021)
14. Liu, B., Xue, L., Fan, H., Ding, Y., Imran, M., Wu, T. An efficient and general automated power amplifier design method based on surrogate model assisted hybrid optimization technique. *IEEE Trans. Microwave Theory Techn.*, **73**, 926–937 (2025)
15. Ma, L., Jin, J., Li, X., Liu, W., Ma, K., Zhang, Q.-J. Advanced surrogate-based EM optimization using complex frequency domain em simulation-based neuro-TF model for microwave components. *IEEE Trans. Microwave Theory Techn.*, **73**, 2309–2319 (2025)
16. Koziel, S., Pietrenko-Dabrowska, A., Machine-learning-based global optimization of microwave passives with variable-fidelity EM models and response features. *Sc. Rep.*, 14, paper no. 6250 (2024)
17. Pietrenko-Dabrowska, A., Koziel, S., Golunski, L. Cost-efficient globalized parameter optimization of microwave components through response-feature surrogates and nature-inspired metaheuristics. *IEEE Access*, **12**, 79051–79065 (2024)
18. Prado, D.R., Naseri, P., López-Fernández, J.A., Hum, S.V., Arrebola, M. Support vector regression-enabled optimization strategy of dual circularly-polarized shaped-beam reflectarray with improved cross- polarization performance. *IEEE Trans. Ant. Propag.*, **71**, 497–507 (2023)
19. Manfredi, P., Probabilistic uncertainty quantification of microwave circuits using Gaussian processes. *IEEE Trans. Microwave Theory Techn.*, **71**, 2360–2372 (2023)
20. Liu, Y., Chen, P., Tian, J., Xiao, J., Noghanian, S., Ye, Q. Hybrid ANN-GA optimization method for minimizing the coupling in MIMO antennas. *AEU – Int. J. Electronics Comm.*, **175**, paper no. 155068 (2024)
21. Tan, J., Shao, Y., Zhang, J., Zhang, J. Efficient antenna modeling and optimization using multifidelity stacked neural network. *IEEE Trans. Antennas Propag.*, **72**, 4658–4663 (2024)

ICCS Camera Ready Version 2026
To cite this paper please use the final published version:
DOI: 10.1007/978-3-032-29909-3_11

22. Liu, J.P., Wang, B.Z., Chen, C.S., Wang, R. Inverse design method for horn antennas based on knowledge-embedded physics-informed neural networks. *IEEE Antennas Wireless Propag. Lett.*, **23**, 1665–1669 (2024)
23. Pang, Y., Zhou, B., Nie, F. Simultaneously learning neighborship and projection matrix for supervised dimensionality reduction. *IEEE Trans. Neural Networks and Learning Syst.*, **30**, 2779–2793 (2019)
24. Müller, D., Soto-Rey, I., Kramer, F. An analysis on ensemble learning optimized medical image classification with deep convolutional neural networks. *IEEE Access*, **10**, 66467–66480 (2022)
25. Jin, J., Feng, F., Zhang, J., Yan, S., Na, W., Zhang, Q. A novel deep neural network topology for parametric modeling of passive microwave components. *IEEE Access*, **8**, 82273–82285 (2020)
26. Yücel, A.C., Bağcı, H., Michielssen, E. An ME-PC enhanced HDMR method for efficient statistical analysis of multiconductor transmission line networks. *IEEE Trans. Comp. Packaging and Manufacturing Techn.*, **5**, 685–696 (2015)
27. Koziel, S., Pietrenko-Dabrowska, A., Expedited variable-resolution surrogate modeling of compact microwave passives in confined domains. *IEEE Trans. Microwave Theory Techn.*, **70**, 4740–4750 (2022)
28. Koziel, S., Pietrenko-Dabrowska, A. Performance-driven surrogate modeling of high-frequency structures, Springer, New York (2020)
29. Koziel, S., Calik, N., Mahouti, P., Belen, M.A. Accurate modeling of antenna structures by means of domain confinement and pyramidal deep neural networks. *IEEE Trans. Ant. Prop.*, **70**, 2174–2188 (2022)
30. Morris, M.D., Factorial sampling plans for preliminary computational experiments, *Technometrics*, **33**, 161–174 (1991)
31. Iooss, B., Lemaitre, P., A review on global sensitivity analysis methods, in G. Dellino and C. Meloni (Eds.) *Uncertainty management in simulation-optimization of complex systems*, 101–122, Springer, New York (2015)
32. Tian, W., A review of sensitivity analysis methods in building energy analysis, *Renewable and Sustainable Energy Rev.*, **20**, 411–419 (2013)
33. Saltelli, A., Making best use of model evaluations to compute sensitivity indices, *Com. Physics. Comm.*, **145**, 280–297 (2002)
34. Jansen, M.J.W., Analysis of variance designs for model output, *Comp. Physics Comm.*, **117**, 25–43 (1999)
35. Kovacs, I., Topa, M., Buzo, A., Rafaila, M., Pelz, G., Comparison of sensitivity analysis methods in high-dimensional verification spaces, *Acta Tecnica Napocensis. Electronics and Telecommunications*, **57**, 3, 16–23 (2016)
36. Koziel, S., Pietrenko-Dabrowska, A., Leifsson, L., Improved efficacy behavioral modeling of microwave circuits through dimensionality reduction and fast global sensitivity analysis, *Sc. Rep.*, **14**, paper no. 19465 (2024)
37. Forrester, A.I.J., Keane, A.J., Recent advances in surrogate-based optimization, *Prog. Aerospace Sci.*, **45**, 50–79 (2009)
38. Tseng, C., Chang, C., A rigorous design methodology for compact planar branch-line and rat-race couplers with asymmetrical T-structures. *IEEE Trans. Microwave Theory Techn.*, **60**, 2085–2092 (2012)
39. Lin, Z., Chu, Q.-X., A novel approach to the design of dual-band power divider with variable power dividing ratio based on coupled-lines. *Prog. Electromagn. Res.*, **103**, 271–284 (2010)

ICCS Camera Ready Version 2026
To cite this paper please use the final published version:
DOI: 10.1007/978-3-032-29909-3_11